

Experimental and numerical investigation of OH* chemiluminescence in shock tubes: Reactions of highly diluted H₂/O₂ mixtures with various diluents

M. Bozkurt^{*1}, M. Hartmann¹, T. Kathrotia², U. Riedel², M. Fikri¹, C. Schulz¹

¹ IVG, Universität Duisburg-Essen, Duisburg, Germany

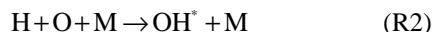
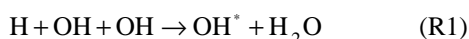
² IWR, Universität Heidelberg, Germany

Abstract

The temporal variation of OH* chemiluminescence in hydrogen oxidation chemistry has been studied behind reflected shock waves at temperatures of 1100–3000 K, at a pressure of 1 bar. The aim of the present work was to obtain a validated reaction scheme to describe OH* formation. The main pathway of OH* formation in hydrogen oxidation at the measured temperature is attributed to $\text{H} + \text{O} + \text{M} \rightarrow \text{OH}^* + \text{M}$ with a derived rate coefficient of $1.5 \times 10^{13} \exp(-25 \text{ kJmol}^{-1}/RT) \text{ cm}^6 \text{ mol}^{-2} \text{ s}^{-1}$. The numerical simulation allows the qualitative analysis for the absolute OH* concentration based on laminar flame data from the literature.

Introduction

In H₂/O₂ combustion, emission of UV radiation at a wavelength of 306 nm in the flame spectra is observed due to the transition of the hydroxyl radical from its electronically excited state (A²Σ⁺) to its ground state (X²Π). The concentration of OH* is much lower (as much as several orders of magnitude) than some of the important ground state intermediate species (OH, H, O) and thus has nearly no influence on the overall hydrogen oxidation. A quantitative interpretation of this signal would be attractive as a cost-efficient optical diagnostic technique of transient combustion phenomena. There is, however, no direct relationship between the measured OH* intensity and the absolute concentration of the important (ground state) flame intermediates. To connect both requires the knowledge of the detailed chemistry of the system involving OH*. While the kinetics of ground state hydroxyl radicals are well known, only few direct measurements of the OH* formation routes exist. Disagreement still remains in defining the main channel forming OH*:



Recent studies [1,2] describe (R2) as the key reaction pathway. The present study focuses on the formation pathway of OH* and the influence of different collision partners based on an existing mechanism of hydrogen oxidation [3] blended by a sub mechanism, containing the kinetics data of the OH* chemistry [4-6]. Here, the rate of the key reaction (R2) is suggested in the present work. The mechanism for OH* chemiluminescence is validated against the ignition delay time measurements from shock-tube experiments for different fuel stoichiometry (present work) and absolute concentration measurements from premixed laminar flames (Smith et al. [2]). The ignition delay calculations are based on a zero-dimensional (0-D) well-stirred reactor model.

The shock-tube technique allows the investigation of OH* chemiluminescence over a wide temperature and

pressure range under defined, ideal conditions, where reactions are considered diffusion-free. This approach has been established to investigate reactions kinetics at high temperature

Experimental

The detection of the OH* chemiluminescence signals were performed in an high-vacuum shock tube with a constant inner diameter of 80 mm. Mixtures were prepared in a stainless steel vessel using the partial pressure method. Stated chemical purities were 99.998% for oxygen, 99.9990% for hydrogen, 99.996% nitrogen and 99.9990% for argon.

The tube is separated into a driver and driven section by an aluminium diaphragm. The driver section with a length of 3.6 m is pumped down to 10⁻² mbar. A final pressure of 10⁻⁷ mbar in the driven section (length: 7.3 m) is achieved by a turbomolecular pump. Hydrogen is used as driver gas. The shock tube provides a test time of 2 ms. Figure 1 shows a schematic setup of the shock tube.

Four piezoelectric pressure transducers are used to record the pressure trace in order to determine the incident shock wave velocity. Temperature and pressure of the test gas behind the reflected shock wave were calculated based on the initial temperature and pressure, the incident shock velocity and the attenuation using a one-dimensional shock tube model (shock-tube code of the CHEMKIN package [7]).

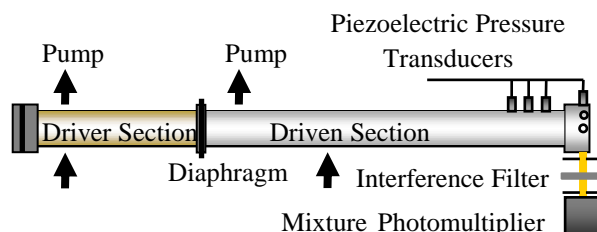


Figure 1: Schematic setup of the shock tube

For the optical detection of the OH* chemiluminescence UV-transparent windows (LiF) are positioned 28 mm upstream of the end flange. A combination of

¹* Corresponding author: metehan.bozkurt@uni-due.de
Proceedings of the European Combustion Meeting 2009

two slits (width: 0.2 mm, distance: 25 mm) narrows the detection volume in order to ensure high temporal resolution. Hence, a time resolution of 4 μs was achievable. An interference filter limits the detected radiation at 307 ± 10 nm (FWHM) to record emission from the $A^2\Sigma^+ \rightarrow X^2\Pi$ transitions of the OH^* radical. The signal is gained by a photomultiplier (Hamamatsu 1P28) with a constant amplification voltage and constant optical configuration during the experimental series. Table 1 shows the investigated mixture compositions for a defined temperature and pressure range.

Table 1: Composition of the mixtures investigated in the present study

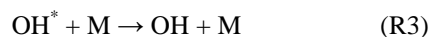
Mixture	ϕ	Composition	T_5 / K	p_5 / bar
A	0.5	1% H_2 + 1% O_2 in Ar	1100 – 3100	0.85 – 1.40
B	1	2% H_2 + 1% O_2 in Ar	1100 – 3100	0.85 – 1.40
C	0.5	1% H_2 + 1% O_2 + 5% N_2 in Ar	1100 – 3100	0.90 – 1.30
D	1	2% H_2 + 1% O_2 + 5% N_2 in Ar	1200 – 3100	0.90 – 1.35

Chemical reaction model

To interpret the data a kinetic model for OH^* chemiluminescence was considered which includes reactions forming and consuming OH^* and a complete hydrogen oxidation mechanism. The entire mechanism considered in the present work is summarized in Table 2. The basic mechanism of hydrogen oxidation, which consists of 10 species and 46 reactions, is adopted from the Warnatz mechanism [3]. It includes temperature as well as pressure-dependent reactions and is recently documented in [8]. The rates of the elementary reactions are based on the recommendations of Baulch et al. (2005) [9]. This mechanism is well validated with respect to flame velocity (5–70% fuel condition) and ignition delay times in the temperature range from 1000–3000 K. The absolute concentrations of the major species (H_2 , O_2 , H_2O , H , OH , O) are in very good agreement with experimental concentrations (not presented in this work).

Results and Discussion

For the calibration of measured signal intensities in terms of OH^* concentration measured signals and simulated concentrations are related to each other at reaction temperatures of 3100 K. For temperatures higher than 3100 K OH^* chemiluminescence can be attributed to the reverse reaction of the collisionally-induced deactivation reaction, i.e.:



The temperature 3100 K represents a transition point where the main reaction pathways (R2, R3) forming OH^* species interchange their importance. Because the reaction (R2) is well known from literature, it can be used for calibration purposes. Figure 2 shows the de-

tected OH^* emission signal and the computed profile for a stoichiometric hydrogen/oxygen mixture at $T = 1607$ K and $p = 1.4$ bar. The OH^* experimental profiles were simulated using the mechanism discussed in the previous section. The profiles of the measured and computed OH^* chemiluminescence are normalized for comparison to their peak values. The shape of the computed profile is well reproduced when compared to the experiment.

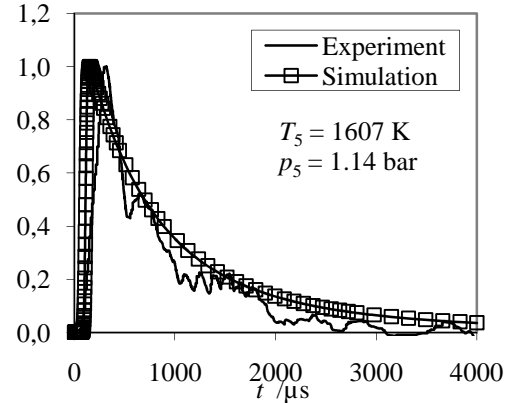


Figure 2: Comparison of the OH^* chemiluminescence shock tube emission profile I_{OH^*} with the simulated OH^* concentration for the mixture composition B. The profiles are normalized to their respective peak values. The simulation is performed with the rate coefficient of reaction (R2) suggested in the present work.

Figure 3 shows the maximum OH^* concentration as a function of temperature of one of the chosen mixture D (for composition see Table 1). The experimental data are shown as closed symbols where the intensity $I_{\text{OH}^*, \text{max}}$ at the given temperature is normalized to the corresponding value at 3100 K for the reason explained above. At the same conditions the simulations (open symbols) are performed and normalized to the concentrations at 3100 K (i.e., $[\text{OH}^*]_{\text{max}}/[\text{OH}^*]_{\text{max}, 3100 \text{ K}}$). The figure shows also the results of the calculation by taking into account different values for the reaction (R2). A frequency factor equal to $1.5 \times 10^{13} \text{ cm}^6 \text{ mol}^{-2} \text{ s}^{-1}$ combined with an activation energy of 25 kJ mol^{-1} yields the best agreement with the experimental findings.

Additionally, results of the ignition delay times from shock-tube studies and the simulations are compared. In the present work the ignition delay time (τ) corresponds to the time when the tangent to maximum slope of OH^* profile intersects the time axis. Calculation of ignition delay times are performed for the given set of experimental conditions for H_2/O_2 mixtures diluted in argon and nitrogen (Table 1). The experimental data correspond to lean ($\phi = 0.5$) and stoichiometric fuel conditions. In the experiments the reflected shock temperature T_5 ranges from 1100–3000 K with pressure p_5 ranging from 0.85 to 1.40 bar.

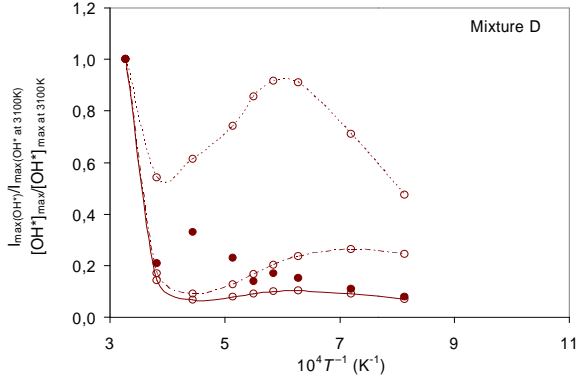


Figure 3: Peak OH* emission $I_{(\text{OH}^*,\text{max})}$ (shock-tube experiment) and molar concentration $[\text{OH}^*]_{\text{max}}$ (simulation) as a function of temperature for mixture D. Experimental and numerical data are normalized to the corresponding values at 3100 K. Closed symbols represent experimental data. Open symbols represent the simulations at corresponding experimental points with varying the rate of reaction (R2) k_2 from present work (—); Hall et al. [1] (---); Smith et al. [4] (-.-). For the chemical composition see Table 1.

Figure 4 shows the comparison of simulated and experimental ignition delay times at above mentioned conditions. The simulations are performed at the given experimental points shown by open symbols. As can be seen from Figure 4, the simulated ignition times are in very good agreement with the measurements at corresponding conditions. The ignition delay times obtained from Ar-diluted mixtures are very close to each other. The variation of diluents shows no effect on the ignition delay (result of N_2 dilution not shown here).

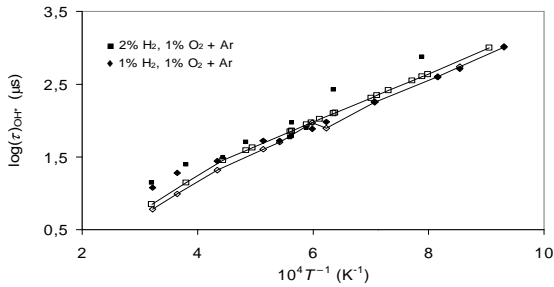


Figure 4: Ignition delay time (τ) with respect to $[\text{OH}^*]$ for stoichiometric and lean H_2/O_2 mixtures with Ar-dilution. Closed symbols: Shock-tube experiments from the present work, open symbols with line: Simulations performed at the given experimental conditions

To validate this finding an additional numerical calculation was done with the maximum intensity plotted against the temperature. The data originates from Hall et al. [1]. Here, similarly to our experiment, the OH* emission profiles using H_2/O_2 mixtures at 0.97 bar were recorded from the side-wall of a stainless shock-tube facility. As given in [1] the data are normalized to a reference temperature at 1490 K. The simulation was

conducted with the derived rate coefficient k_2 discussed in the previous section. The computed normalized OH* signals to the temperature reference (1490 K) shows a good agreement with the experimental data using the rate coefficient suggested above.

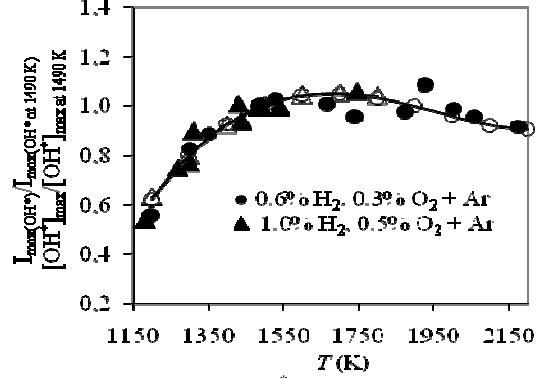


Figure 5: Peak value of OH* emission $I_{\text{max}(\text{OH}^*)}$ (experimental data from [1]) and molar concentration $[\text{OH}^*]_{\text{max}}$ (simulation) at given temperatures normalized to the corresponding value 1490 K for a stoichiometric H_2/O_2 mixture at 0.97 bar. Closed symbols: Experiments from Hall et al. [1]. Open symbols: Simulation done at corresponding conditions with the rate of reaction (R2) derived in the present work.

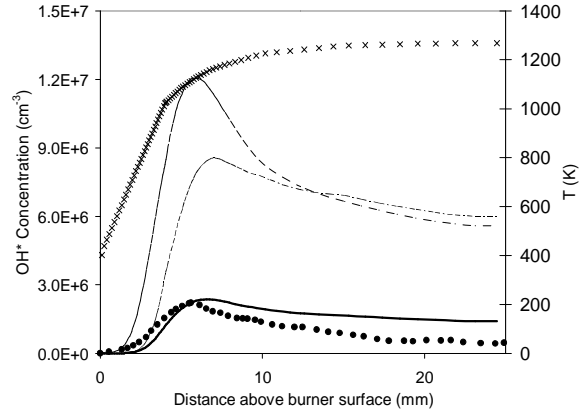


Figure 6: Absolute OH* concentration obtained for a rich ($\phi = 1.54$), low pressure (0.05 bar), laminar premixed H_2 -air flame. \times Temperature profile; \bullet $[\text{OH}^*]$ from experiment, [2]; \circ $[\text{OH}^*]$ from simulation with k_2 from: ----: Smith et al. [2]; -.-: Hall et al. [1]; —: present work.

Additionally, a 1-D laminar premixed low-pressure flame calculation was performed to get insight into the species responsible for the OH* formation chemistry and where data are available. Absolute concentrations in flame provide an astringent test for the elaborated kinetic model. Moreover, ground states chemistry is influential to the OH* formation. Therefore, literature data of Vandooren et al. [10] were taken into account to verify the model.

Table 2: Reaction kinetic scheme of hydrogen oxidation along with OH* sub-scheme.

Elementary reaction	$A / \text{cm mol s}$	n	E / kJmol^{-1}	Reference
H₂/O₂ kinetic scheme				
O ₂ + H = OH + O	2.06E+14	-0.097	62.85	[9]
H ₂ + O = OH + H	3.82E+12	0.0	33.26	[9]
H ₂ + OH = H ₂ O + H	2.17E+08	1.52	14.47	[9]
OH + OH = H ₂ O + O	3.35E+04	2.42	-8.06	[9]
H + H + M(1) = H ₂ + M(1)	1.02E+17	-0.6	0.00	[9]
O + O + M(1) = O ₂ + M(1)	5.40E+13	0.0	-7.40	[8]
H + OH + M(2) = H ₂ O + M(2)	5.56E+22	-2.0	0.00	[9]
H + O ₂ + M(3) = HO ₂ + M(3)	1.75E+17	0.0	0.00	[9]
HO ₂ + H = OH + OH	4.46E+14	0.0	5.82	[9]
HO ₂ + H = H ₂ + O ₂	1.05E+14	0.0	8.56	[9]
HO ₂ + H = H ₂ O + O	1.44E+12	0.0	0.00	[9]
HO ₂ + O = OH + O ₂	1.63E+13	0.0	-1.86	[9]
HO ₂ + OH = H ₂ O + O ₂	9.28E+15	0.0	73.25	[9]
HO ₂ + HO ₂ = H ₂ O ₂ + O ₂	4.22E+14	0.0	50.14	[9]
OH + OH + M(1) = H ₂ O ₂ + M(1)	1.57E+13	0.0	0.00	[9]
H ₂ O ₂ + H = H ₂ + HO ₂	1.69E+12	0.0	15.71	[9]
H ₂ O ₂ + H = H ₂ O + OH	1.02E+13	0.0	14.97	[9]
H ₂ O ₂ + O = OH + HO ₂	4.22E+11	0.0	16.63	[9]
H ₂ O ₂ + O = H ₂ O + O ₂	4.22E+11	0.0	16.63	[9]
H ₂ O ₂ + OH = H ₂ O + HO ₂	1.64E+18	0.0	123.05	[9]
OH* sub-scheme				
H + O + M(1) = M(1) + OH*	1.50E+13	0.0	25.0	present work
OH* = OH + $h\nu$	1.45E+06	0.0	0.0	[4]
OH* + O ₂ = OH + O ₂	2.10E+12	0.5	-2.0	[5]
OH* + H ₂ O = OH + H ₂ O	5.93E+12	0.5	-3.6	[5]
OH* + H ₂ = OH + H ₂	2.95E+12	0.5	-1.9	[5]
OH* + N ₂ = OH + N ₂	1.08E+11	0.5	-5.2	[5]
OH* + OH = OH + OH	6.01E+12	0.5	-3.2	[5]
OH* + H = OH + H	1.31E+13	0.5	-0.7	[5]
OH* + Ar = OH + Ar	1.69E+12	0.0	17.3	[6]

$k = AT^n \exp(-E/RT)$. Efficiencies of colliders are given below:

$$M(1) = [\text{H}_2] + 6.5[\text{H}_2\text{O}] + 0.4[\text{O}_2] + 0.35[\text{Ar}]$$

$$M(2) = [\text{H}_2] + 2.5[\text{H}_2\text{O}] + 0.4[\text{O}_2] + 0.15[\text{Ar}]$$

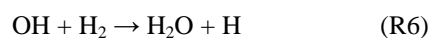
$$M(3) = [\text{H}_2] + 6.5[\text{H}_2\text{O}] + 0.4[\text{O}_2] + 0.29[\text{Ar}]$$

Furthermore, taking the recommended rate of reaction (R2) into account, the absolute peak OH* concentration was also found in good agreement with the number density of OH* measured in premixed flames by Smith et al. [2] by measuring absolute chemiluminescence yields at 310 and 430 nm. The results are shown in Figure 6. The shape of the measured OH* concentra-

tion as a function of distance above the burner surface is reasonably well predicted by the numerical analysis.

A global sensitivity analysis for the laminar flame as well as for the shock tube was performed. The basic step $\text{O}_2 + \text{H} \rightarrow \text{OH} + \text{O}$ (R4) was found to be the most sensitive either for stoichiometric and fuel-rich conditions. Furthermore other reactions were found to have

significant sensitivity from the analysis. The reaction kinetics of OH^* was determined by the important chain branching reaction (R4) along with reactions (R5), (R6) and (R7).



Conclusion

Based on shock tube and laminar premixed flame experiments OH^* chemiluminescence behavior is reproduced by a numerical reaction mechanism. The major channel of excited hydroxyl radical formation is found to be $\text{H} + \text{O} + \text{M} \rightarrow \text{OH}^* + \text{M}$. A reaction coefficient of $1.5 \times 10^{13} \exp(-25 \text{ kJmol}^{-1}/RT) \text{ cm}^6 \text{ mol}^{-2} \text{ s}^{-1}$ is suggested. A sensitivity analysis points out the importance of the basic chain branching $\text{O}_2 + \text{H} \rightarrow \text{OH} + \text{O}$ for the OH^* formation. Simulations of OH^* concentrations based on the kinetic data and flame measurements from literature compare well.

Acknowledgements

The authors are grateful to Prof. Ulrich Maas (University of Karlsruhe) for providing us with his INSFLA code. The financial support from the Deutsche Forschungsgemeinschaft (German Research Foundation, DFG) is gratefully acknowledged.

References

1. J.M. Hall, E.L. Petersen, *Int. J. Chem. Kin.* 38 (2006) 714-724.
2. G. Smith, C. Park, J. Luque, *Combust. Flame* 140 (2005) 385-389.
3. J. Warnatz, U. Maas, R.W. Dibble, *Combustion*, 4 ed (Springer-Verlag, Berlin Heidelberg, New York, 2006).
4. G. Smith, J. Luque, C. Park, J. Jeffries, D. Crosley, *Combust. Flame* 131 (2002) 59-69.
5. M. Tamura, B. Pamela, J. Harrington, J. Luque, J. Jeffries, G. Smith, D. Crosley, *Combust. Flame* 114 (1998) 502-514.
6. P. Paul, J. Durant, J. Gray, *J. Chem. Phys.* 102 (1995)
7. R.J. Kee, F.M. Rupley, J.A. Miller, M.E. Coltrin, J.F. Grcar, E. Meeks, H.K. Moffat, A.E. Lutz, G. Dixon-Lewis, M.D. Smooke, J. Warnatz, G.H. Evans, R.S. Larson, R.E. Mitchell, L.R. Petzold, W.C. Reynolds, M. Carcotsis, W.E. Stewart, P. Glarborg, C. Wang, O. Adigun, CA (2000)
8. C. Heghes. 2007, University of Heidelberg: <http://reaflow.iwr.uni-heidelberg.de/doctoral.html>.
9. D.L. Baulch, C.T. Bowman, C.J. Cobos, R.A. Cox, T. Just, J.A. Kerr, M.J. Pilling, D. Stocker, J. Troe, W. Tsang, R.W. Walker, J. Warnatz, *J. Phys. Chem. Ref. Data* 34 (2005) 757-1397.
10. T. Vandooren, J. Bian, *Proc. Comb. Symp.* 23 (1990) 341-346.